Journal of Nuclear Materials 513 (2019) 282–292

Contents lists available at ScienceDirect

Journal of Nuclear Materials

journal homepage: www.elsevier.com/locate/jnucmat

Corrosion characteristics of copper in static liquid lithium under high vacuum

X.C. Meng [a, b], C. Xu [c], G.Z. Zuo [d], M. Huang [d], K. Tritz [e], D. Andruczyk [f], Z. Sun [d], W. Xu [a, b], Y.Z. Qian [d], J.J. Huang [a], X. Gao [d], B. Yu [b], J.G. Li [d], J.S. Hu [d, g, *], Huiqiu Deng [c, **]

[a] Advanced Energy Research Center, Shenzhen University, Shenzhen, 518060, People's Republic of China
[b] Key Laboratory of Optoelectronic Devices and Systems of Ministry of Education and Guangdong Province, College of Optoelectronic Engineering, Shenzhen University, Shenzhen, 518060, China
[c] Department of Applied Physics, School of Physics and Electronics, Hunan University, Changsha, 410082, China
[d] Institute of Plasma Physics, Chinese Academy of Sciences, Hefei, 230031, China
[e] Johns Hopkins University, Baltimore, MD, 21211, USA
[f] Center for Plasma Material Interactions, Department of Nuclear, Plasma and Radiological Engineering, University of Illinois Urbana-Champaign, Urbana, IL, 61801, USA
[g] CAS Key Laboratory of Photovoltaic and Energy Conservation Materials, Hefei, 230031, China

ARTICLE INFO

Article history:
Received 5 July 2018
Received in revised form
23 October 2018
Accepted 23 October 2018
Available online 25 October 2018

ABSTRACT

Copper (Cu) materials are extensively used as heat sinks and sealing gaskets in fusion devices because they have the properties of good thermal and electrical conductivity and high plasticity. Meanwhile, liquid lithium (Li) is considered as a potential blanket coolant and tritium breeder and/or plasma facing material in fusion devices. Studying the corrosion characteristics of Cu materials by liquid Li under extreme fusion conditions is important because the corrosion of Cu by liquid Li may affect simultaneous application of these materials in fusion devices. The corrosion behavior of Cu in static liquid Li at 620 K for 15 h under high vacuum was investigated. After exposure to liquid Li, the weight loss rate of Cu in liquid Li is 466.1 $g\,m^{-2}\,h^{-1}$, which is equivalent to 458.7 $mm\cdot a^{-1}$ for the average corrosion depth rate. The entire surface of each specimen was seriously damaged. Visible grain boundary corrosion was observed on the surface of the specimens. Also, Cu debris entered the liquid Li from the corroded surface, resulting in considerable Cu loss from the specimen. These results demonstrate a corrosion protection grade of Cu in liquid Li of 10, Cu cannot withstand the corrosion of liquid Li under the given conditions. Additionally, the corrosion process of Cu in liquid Li at 620 K under high vacuum was studied using the Large-scale Atomic/Molecular Massively Parallel Simulator (LAMMPS). The results from these simulations indicate that the corrosion of Cu in liquid Li is induced via physical dissolution and intergranular corrosion, where intergranular corrosion is the dominant mechanism.

1. Introduction

Cu and Cu alloys are some of the most widely used metals due to their excellent heat conductivity, electrical conductivity, machinability, and welding properties. Therefore, these metals have many applications as thermally conductive and conductive materials, and even structural materials in industry and in our daily life, such as in heat exchangers, tubes, cables, electrical wiring, switching devices and transformers, etc … [1]. Furthermore, Cu and Cu alloys are play an important role in fusion devices, and are extensively used as materials for sealing gaskets, heat sinks, and tungsten/copper (W/Cu) divertor assemblies. By using Cu sealing gaskets, which have high plasticity and can withstanding high-temperature, devices can bake to a higher temperature and pump down to a higher quality vacuum [2]. Additionally, CuCrZr alloys are being considered as a primary candidate for the first wall heat sink material due to their high heat conductivity and high mechanical strength [3–6]. For the Experimental Advanced Superconducting Tokamak (EAST) device, a

* Corresponding author. Institute of Plasma Physics, Chinese Academy of Sciences, Hefei, 230031, China.
** Corresponding author. Department of Applied Physics, School of Physics and Electronics, Hunan University, Changsha, 410082, China
E-mail addresses: hujs@ipp.ac.cn (J.S. Hu), hqdeng@hnu.edu.cn (H. Deng).

https://doi.org/10.1016/j.jnucmat.2018.10.037
0022-3115/

CuCrZr alloy is used as a structural material for actively cooled plasma facing components (PFCs). The PFC support structures are made of CuCrZr on which the plasma facing tiles are mechanically attached [7]. There are several Cu tubes deployed along channels located behind the PFC heat sink. During vacuum testing and vessel bake-out, hot nitrogen gas flows through the tubes to heat the components to a sufficient temperature to drive out water vapor and other residual gases. Alternatively, during plasma operation the Cu tubes will transport water to cool the heat sink and tiles [8]. In 2006, a W/Cu limiter (W coating on a Cu heat sink) was tested on HT-7 as an actively water-cooled, movable limiter, and was subjected to ~40 discharges with estimated local heat fluxes up to 10 MWm^{-2} [9]. In 2014, EAST changed the graphite upper divertor to a W/Cu upper divertor for facilitating long-pulse operations [10]. It is evident that Cu and Cu alloys have played, and will continue to play a critical role in fusion experimental devices. Therefore, the compatibility and general interaction of Cu with newly considered materials, such as liquid Li, is of general interest and importance.

Liquid Li is a novel material which has received increased attention in recent decades due to its interesting physical and chemical properties. Blanket concepts using liquid Li as both a coolant and breeder material are an attractive option that provide high thermal conductivity and high tritium breeding efficiency [11,12]. In fusion devices with a liquid Li plasma facing surface [13–17], significant improvements of plasma performance have been observed, e.g. plasmas with lower recycling, reduced impurity levels and higher confinement have been achieved. In addition to improved plasma performance, liquid lithium PFCs are an attractive option with respect to handling the high heat flux from plasma exhaust. During plasma discharges, when conventional solid PFCs are exposed to high heat loads, they can suffer from several forms of damage, such as blistering, cracking, and melting. However, liquid Li walls can withstand these high heat loads and particle fluxes, thus protecting the underlying solid substrates [18]. Therefore, liquid Li is now being considered as a potential candidate material for PFCs for both the first wall as a limiter/divertor in fusion devices. In 2014, a new flowing liquid Li limiter (FLiLi) with temperature of about 350 °C based on the concept of a thin flowing film has been successfully tested in the EAST device [19]. Nevertheless, after the conclusion of the experiment, it was found that the surface of FLiLi was damaged by the bombardment of high-energy particles and the Cu heat sink was corroded by liquid Li.

In this instance, the liquid Li most likely infiltrated and contacted the Cu material through the cracks and gaps of components. If liquid Li is used as material component of the blanket and/or first wall in future fusion devices, it will be important to understand the detailed interactions of liquid Li and Cu, which may significantly affect the application and simultaneous use of those two materials. However, there is a dearth of literature regarding the compatibility of Cu and liquid Li. In consideration of the lifetime of Cu parts and even the safety of fusion devices with the use of liquid Li in fusion environment, the corrosion characteristics of Cu in liquid Li must be well understood. In this paper, the corrosion behavior and processes of Cu in static liquid Li at 620 K under high vacuum are investigated and simulated, the corrosion mechanism is also discussed.

2. Experimental setup

2.1. Materials information

We obtained coupon-type Cu specimens with a purity of 99.95% and dimensions of 30 mm × 15 mm × 3 mm. The surface of these specimens was mechanically polished and cleaned by ultrasound in 99.9% purity alcohol before the experiment. 99.9% purity metallic Li was supplied in the form of ingots. The chemical compositions and ratios of Cu and Li are given in Table 1. The vessel and mounting points of the experiment device are made of 304 stainless steel (304 SS). Nine Cu specimens and 187 g Li were used in the present experiment.

2.2. Experiment device and conditions

Corrosion testing of the Cu specimens was performed in a liquid Li testing device. To reduce the effect of gaseous impurities on the experimental corrosion results, the device is heated to >700 K by a resistive heating element, and is pumped to a vacuum pressure of $<10^{-4}$ Pa using a turbo-molecular pump. The schematic diagram of the experimental device is shown in Fig. 1. Prior to the experiment, nine specimens were attached to the mounting points 20 mm above the bottom of the test vessel. The pressure of the testing device was then pumped to $<10^{-3}$ Pa to prevent the oxidation of Cu specimens when the device was subsequently heated. Following the evacuation of the vessel, the device was heated to 700 K and held at temperature for 12 h to desorb the adsorbed gas on the device wall and Cu surfaces. After the desorption process was complete, ~187 g Li was placed into test vessel, backfilled with argon (Ar) to prevent lithium oxidation. The entire assembly was then heated to 620 K and pumped down to 10^{-4} Pa to begin the experimental corrosion testing. The depth of liquid Li was ~47 mm after the Li was fully melted, with the Cu specimens completely immersed in the liquid Li. After the conclusion of the experiment, liquid Li was protected by Ar and passed to the storage vessel from the test vessel, where the specimens were extracted.

To protect the device safety during operation, a safety interlock and protection system was implemented. If the pressure of the vessel exceeds 10 Pa, an electromagnetic valve will introduce Ar to the system, while another electromagnetic valve will gate off the turbo-molecular pump. This safety system is designed to fill the vessel with 1 atm of Ar, and protect the Li from the risk of fire or explosion.

2.3. Cleaning and testing of specimen

Since the specimens can be damaged by the strong reaction of water and Li [20,21], the corroded specimens were primarily cleaned using high purity ethanol to remove the adhered Li from the Cu surface. For a better understanding of the corrosion behaviors and mechanisms: the weight change of the specimens was measured using an electronic balance with an accuracy of 0.01 mg; metallurgical analysis was performed with the aid of an optical microscope; and the microstructural and compositional information of the specimens was characterized by means a scanning electron microscopy (SEM) equipped with an energy dispersive spectrometer (EDS) and X-ray photoelectron spectroscopy (XPS) before and after the corrosion experiment.

2.4. Simulation details

In order to understand the corrosion processes of Cu in liquid Li and study the diffusion kinetics of Cu and Li atoms in Cu–Li solid-liquid interface, a Cu–Li solid-liquid interface model was established. The corrosion processes of Cu in liquid Li under the experimental environment was then simulated using the LAMMPS [22]. In the present work, the interatomic potential between Cu and Li atoms was developed by our group, and has been successfully used to investigate the wetting properties of Li droplets on Cu surfaces [23]. To construct the Cu–Li solid-liquid sample, the polycrystalline Cu bulk was brought to equilibrium within 0.5 ns using an NPT (constant number of atoms, pressure and temperature) ensemble.

Table 1
The chemical compositions and ratios of Cu and Li.

Li	Composition	Na	K	Ca	Fe	N	Si	Cl	Al	Ni	Cu
	Wt%	0.0045	0.0002	0.0015	0.003	0.0027	0.002	0.002	0.001	0.002	0.001
Cu	Composition	As	S	Fe	Ag	Sn	P	Pb	Ni	O	Cu
	Wt%	0.005	0.0076	0.0063	0.005	0.005	0.0065	0.003	0.0045	0.001	Bal

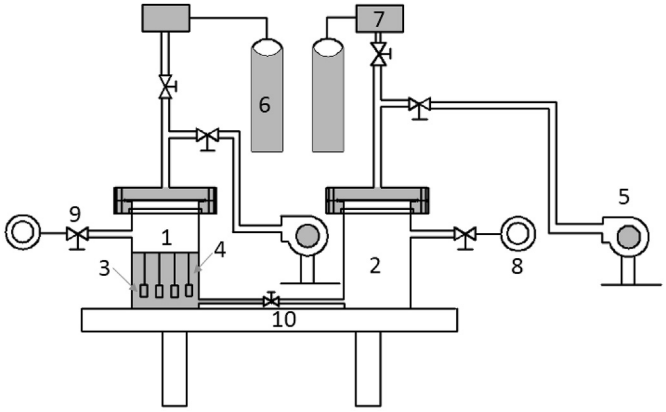

Fig. 1. The schematic diagram of the experimental device. Shown are the (1) test vessel, (2) storage vessel, (3) Cu specimens, (4) liquid Li, (5) turbo-molecular pump, (6) argon, (7) pressure controller, (8) vacuum gauge, (9) valve, (10) supporting platform.

The cross-sectional areas of the solid-liquid interface were determined by the equilibrated Cu bulk, and the liquid Li bulk was constructed via melting solid Li at 620 K. The starting configuration was specified by conjoining the solid Cu and liquid Li samples at their common cross-sections. A common neighbor analysis (CNA) was then performed to identify the solid and liquid structures [24]. The dimensions of the solid-liquid configuration are 163 Å × 163 Å × 348 Å containing a total of 548215 atoms. The CNA result of the solid-liquid system is shown in Fig. 2. All of the simulations were performed by the LAMMPS with a time step of 2.0 fs [22]. The Nose–Hoover thermostat [25,26] and Parrinello–Rahman barostat [27] were adopted to control the temperature and pressure, respectively. All simulations used periodic boundary conditions in all three spatial directions. After the starting configuration was constructed, the solid-liquid model was relaxed over 1.0 ns to simulate the corrosion of solid Cu in liquid Li.

3. Results

3.1. Weight loss of Cu in pure Li

The weight changes for the specimens were obtained using the weight-loss method. Each specimen was measured several times, then the average value was calculated. After exposure to liquid Li for 15 h, the total weight loss of the nine specimens was 85 (±0.00027) g, which is equivalent to 6991.5 g m^{-2}. This corresponds with a weight loss rate of 466.1 g m^{-2} h^{-1}, which is equivalent to 458.7 mm·a^{-1} for the average corrosion depth rate, using the value of 8.9 g cm^{-3} for the density of Cu. These results demonstrate that the “corrosion protection grade” of Cu reaches 10 [28]. The phrase “corrosion protection grade” refers to a material's ability to resist environmental corrosion. There are ten grades of corrosion protection, enumerated from 1 to 10, where the smaller the value, the stronger the corrosion resistance of the material. Thus, these results clearly demonstrate that Cu cannot withstand the corrosion of liquid Li at 620 K under high vacuum.

3.2. Morphology of corroded Cu specimens

After the test vessel was opened, it was discovered that the Cu specimens had fallen to the bottom of the test vessel from the mounting points, as shown in Fig. 3(a). One of the test specimens had completely disappeared, which suggested that large quantities of Cu were corroded and essentially dissolved into the liquid Li. Furthermore, it was also discovered that significant amounts of debris had accumulated on the bottom of the test vessel. After cleaning, both the Cu specimens and collected debris exhibited a metallic luster, while specimens also displayed nonuniform corrosion, as shown in Fig. 3(b) and (c). Five of the specimens were badly corroded by liquid Li: a hole appeared in one of the specimens; three of the specimens were reduced in size to roughly a half-sized block; and one other specimen was completely dissolved in the liquid Li. The remaining four specimens were corroded by varying degrees. After measuring, it was found that the length and width of the these remaining four specimens were reduced by 3–5 mm and 2–3 mm respectively. Finally, the four sides of specimens were measured to be 0.5–1 mm thinner than the measured thickness in the middle.

In order to conveniently describe the morphology of corroded samples, all of the remaining specimens were numbered from 1 to 8, as shown in Fig. 3(b), and the morphology analysis was performed with the aid of an optical microscope and SEM. The measured areas on both sides of the hole which appeared on the specimen number one are 6.5 mm^2 and 4 mm^2. From these results, we can deduce that the edge of the hole is tilted, i.e. it is an inclined

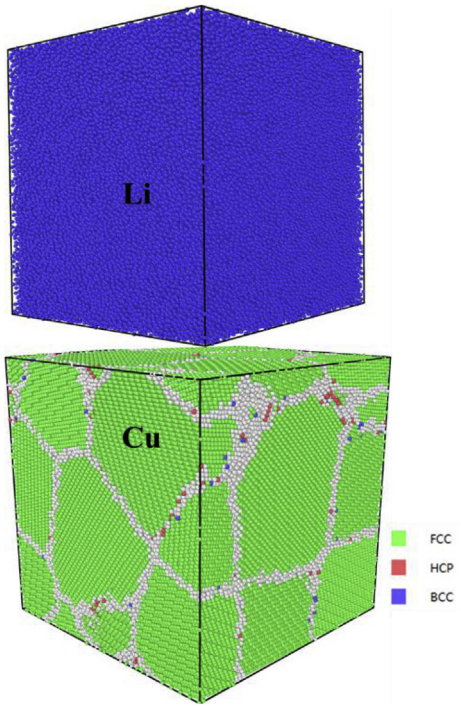

Fig. 2. The CNA results of the starting configuration of the solid-liquid system.

rather than a vertical hole. At a higher magnification of the optical microscope, the shape and tilted edge of the hole can be clearly observed in Fig. 4, which supports this conclusion. Furthermore, a hollow with a funnel shape, as shown in Fig. 5, is found on another side of specimen #5. The Cu layers, which can be distinguished from the whiter Li oxide material, are clearly observed in the tilted edges of the hollow. This suggests that the corrosion process of this hollow can be viewed as a similar mechanism compared to the corrosion process of the hole. As shown in Fig. 3(b), most edges of specimens are corroded to heavily distorted shapes, particularly the #2 and #7 specimens, as shown in Fig. 6(a). Fig. 6 also illustrates a serious corrosion on the surfaces of the specimens. Fig. 6(b) and (c) shows that residual Li and some Cu debris still adhered to the bottom specimen #6, and some adherent debris (remnant layers) were clearly observed on the edges of the specimen.

As shown in Fig. 7(a), prior to the corrosion test, the Cu specimen exhibits a metallic luster and many grooves on the surface from mechanical processing. After exposure to liquid Li, as shown in Fig. 7(b) and 7(e), the grains and grain boundaries of Cu specimens can be observed clearly at higher magnification of the SEM, indicating that the specimens suffered from a distinct grain boundary attack. It is discovered that the surface microstructures are somewhat different with positions on specimen #5. Different areas on the surface of specimen #5 (indicated in Fig. 7(b)) correspond to various size and shapes of grains, shown in Fig. 7(c – e). Furthermore, many of the grains bear cut marks which indicate damage to this area of the specimen. Fig. 7(c) shows a large amount

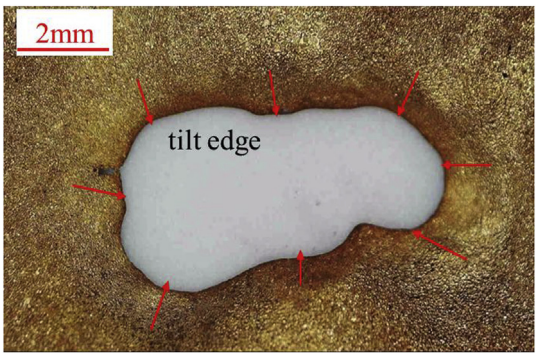

Fig. 4. The shape of the hole in specimen #1.

of grains with diverse size and Fig. 7(d) shows spinel-like located at a different area of the specimen. Additionally, there are pebble shape grains with varying sizes shown in Fig. 7(e), with distinct gaps between grains. At higher magnification, as shown in Fig. 8, one can observe many white precipitates on the grain boundaries. EDS analysis shows the main elements of the precipitates are C, Fe, and Cu, which indicates that the primary composites are Fe carbides. These elements of Fe and C leeched from the 304SS vacuum vessel, formed Fe carbides and adhered to the surface of the Cu specimen. The C is assumed to be dissolved as Li_2C_2 in liquid Li at low concentration of nitrogen [29,30]. The possible chemical

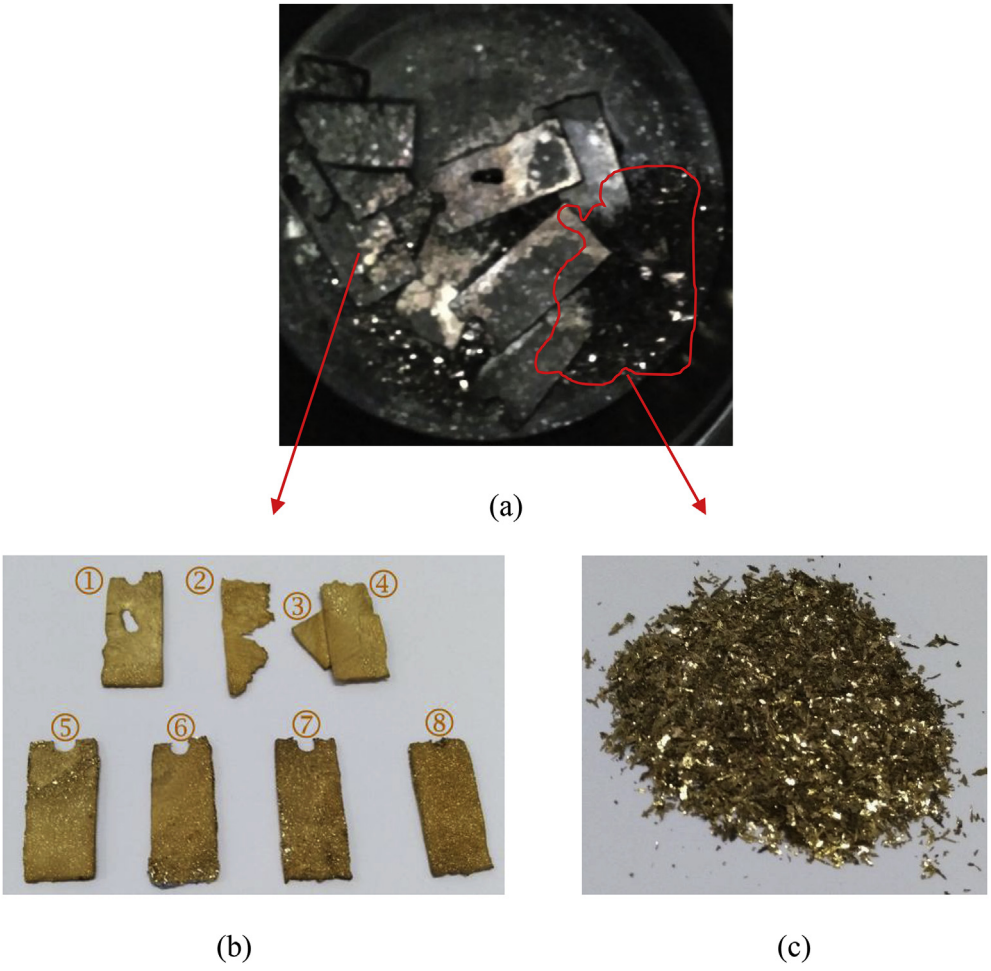

Fig. 3. The morphology of the Cu specimens and debris. (a) bottom picture of the test vessel, (b) specimens show metallic luster while badly corroded, (c) morphology of Cu debris.

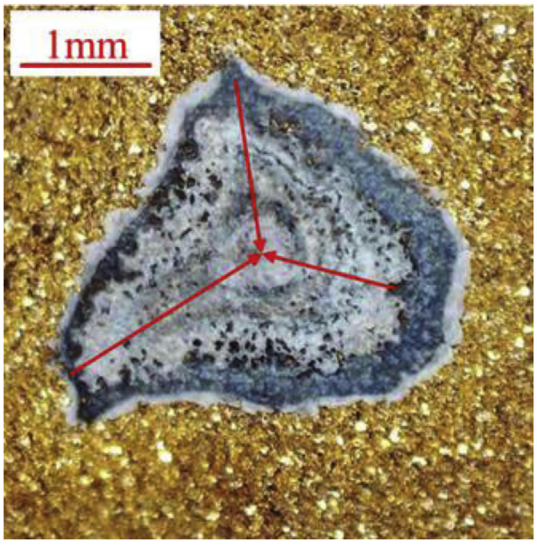

Fig. 5. The morphology of the hollow in specimen #5.

reaction of Fe carbides in liquid Li and/or on the surface of Cu specimen is:

$$6Fe + Li_2C_2 \xrightarrow{\Delta} 2Fe_3C + 2Li \quad (1)$$

the Gibbs free energy of Eq. (1) is about 7.7 kJ/mol at 620K. Then the corrosion production of Fe carbides transferred and adhered to the surface of the Cu specimen. The details of the corrosion behavior of 304SS in static liquid Li were reported in Refs. [31,32].

3.3. Structural morphology of Cu debris

Cu debris was formed with a wide range of disparate sizes from 6 μm to 8 mm, but still demonstrated a metallic luster, as shown in Fig. 3(c). Using microscopic dark field imaging, it was observed that the larger debris displayed spearhead and metasequoia leaf shapes, as shown in Fig. 9(a) and (b). The metallurgical analysis was also performed with the aid of an optical microscope. Fig. 9(c) shows the metallographic structure of the original Cu specimen. Furthermore, through comparison and analysis the both directions of grain boundaries of debris and the metallographic structure of Cu, it was found that the morphologies of the debris are determined by the metallographic structure of Cu. Finally, as shown in Fig. 9(d), the small debris particles exhibited pebble-like shapes with sizes from 5 μm to 20 μm as measured by SEM analysis. As the remnant Li in the storage vessel was cleaned with water, there were remnant buoyant particles that accumulated at the surface of the water, as shown in Fig. 10. After drying, the compositions of these remnant particles were measured using EDS surface analysis. The result of the EDS analysis demonstrated that the main component elements were Cu and O. Furthermore, the XPS analysis revealed that the main composition of the buoyant particles was CuO, as shown in Fig. 11.

3.4. Simulation result

After relaxing the simulation for 1.0 ns, the snapshots of

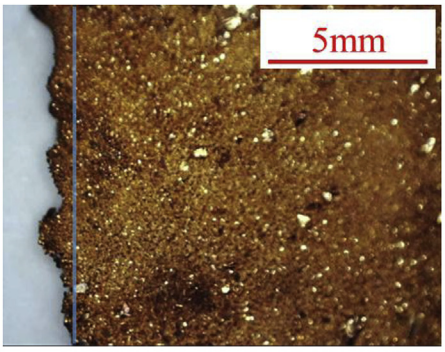

(a)

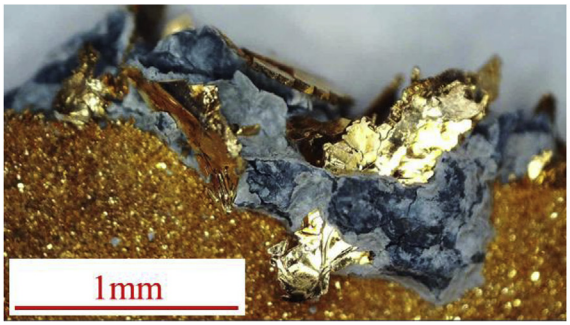

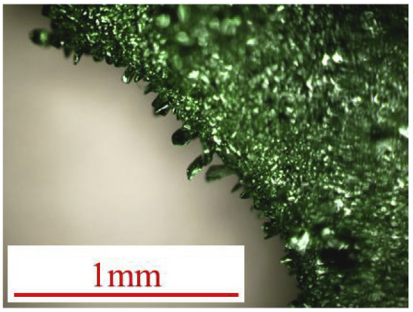

(b) (c)

Fig. 6. The edge shapes of a number of Cu specimens. Shown are the (a) zigzag shape of specimen #7 edge, (b) residual Li including debris still adhered to the bottom of specimen #6, (c) adherent debris observed on the specimen edges using dark field optical microscopy.

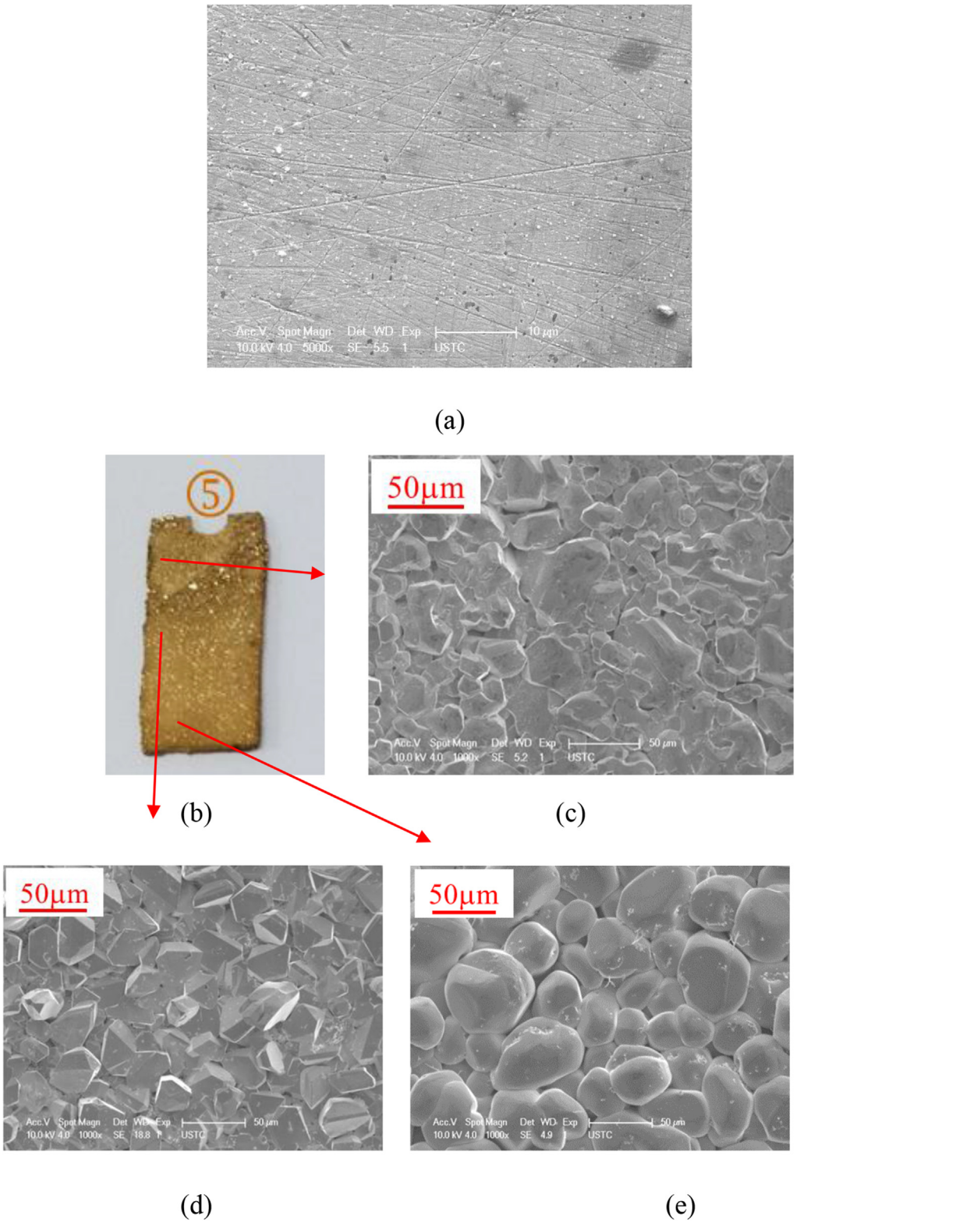

Fig. 7. The microstructure of grains and grain boundaries at different positions. Shown are the (a) initial state of the specimen surface,(b) specimen #5 post-corrosion, (c) various sizes and shapes of Cu grains, (d) spinel-like grains, (e) pebble-shaped grains.

equilibrated solid-liquid system are plotted in Fig. 12. As shown in Fig. 12(a), the liquid Li atoms has permeated into the Cu substrate near the Cu—Li solid-liquid interface, which is a sign of Cu substrate corrosion. To illustrate the result of corrosion more clearly, Fig. 12(b) shows the result of deleting the Li atoms from the output. It can be seen that Cu atoms become distributed throughout the liquid Li, indicating that the Cu atoms become dissolved and diffused in the liquid Li. This is consistent with the experimental

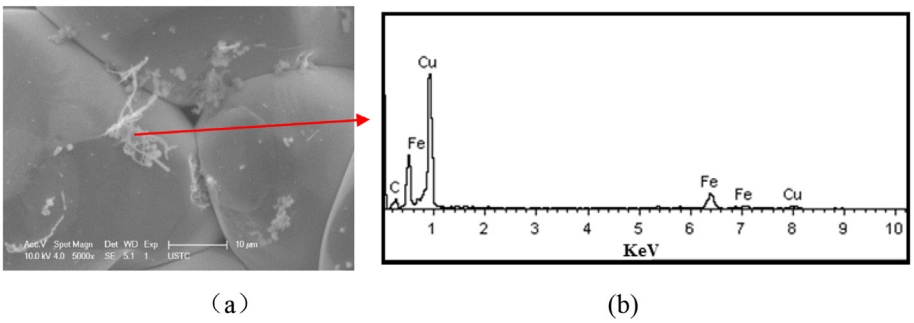

Fig. 8. The microstructure and component analysis of the precipitates. Shown are the (a) white precipitates on the grain boundaries, (b) EDS analysis result of the precipitates.

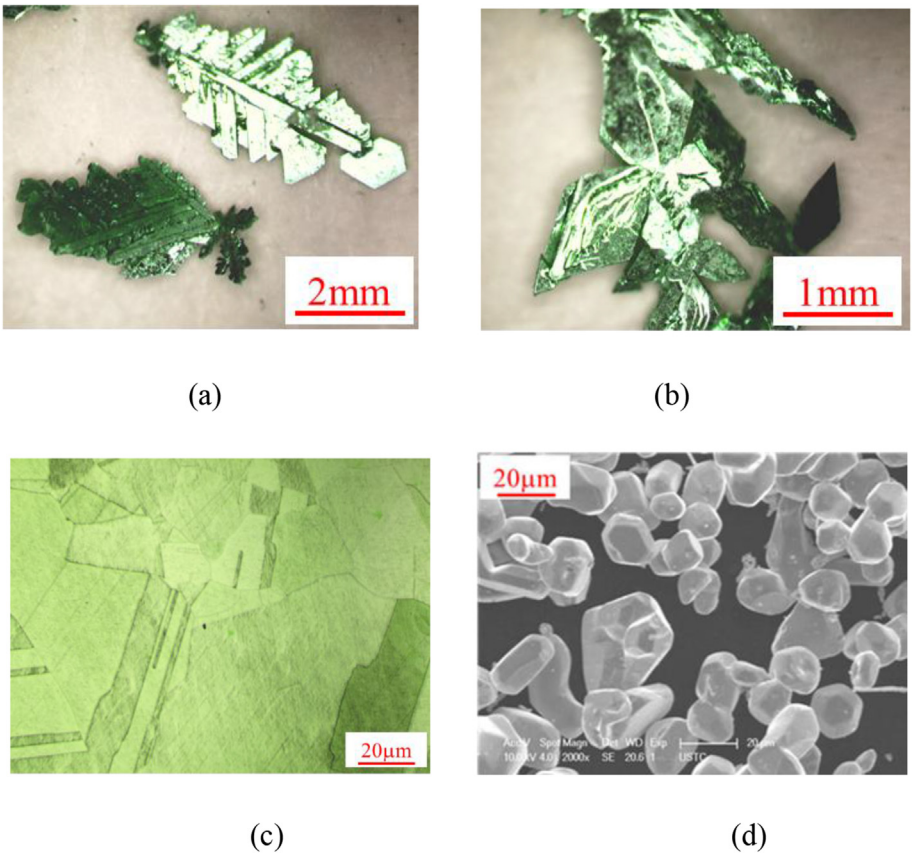

Fig. 9. The microstructure of Cu debris and metallographic structure. Shown are the (a) metasequoia leaf shape debris, (b) spearhead-shape debris, (c) metallographic structure of Cu, (d) pebble-shaped grains.

observations of physical dissolution of the Cu bulk into the liquid Li. Next, the section of Cu substrate is sliced out at the region near the interface to illustrate the simulated morphology of Cu near the solid-liquid interface. In addition, CNA is employed to highlight the morphology of the Cu grain boundaries. The snapshots of the Cu substrate section and the CNA results are respectively shown in Fig. 12(c) and (d). Comparing these two snapshots, it can be determined that the liquid Li atoms in the Cu substrate are primarily distributed around the grain boundary, which suggests that the liquid Li atom atoms enter the substrate through the grain boundary. This supports the experimental observations of grain boundary corrosion as show in Fig. 7. Therefore, the simulation results suggest that the corrosion processes of Cu in liquid Li are composed of the dissolution of Cu atoms and permeation of Li atoms into the substrate.

4. Discussion

Based on the results from the experiment and simulation, it's found that the corrosion mechanisms of Cu in liquid Li under the given conditions of experiment include two main aspects: physical dissolution and intergranular corrosion, with the intergranular corrosion taking the leading role. The corrosion process of Cu in liquid Li contains two stages. A schematic of the corrosion processes of Cu in liquid Li is shown in Fig. 13.

Fig. 13(a) shows the initial sate of Cu specimen and liquid Li, where the specimen is immersed in liquid Li. During the first stage, the Cu atoms dissolve into liquid Li from the specimen near the solid-liquid interface, and gradually diffuse throughout Li, as shown in Figs. 13(b) and 12(b). Additionally, the liquid Li infiltrates into the machine marks and diffuses into the grain boundaries, as shown in

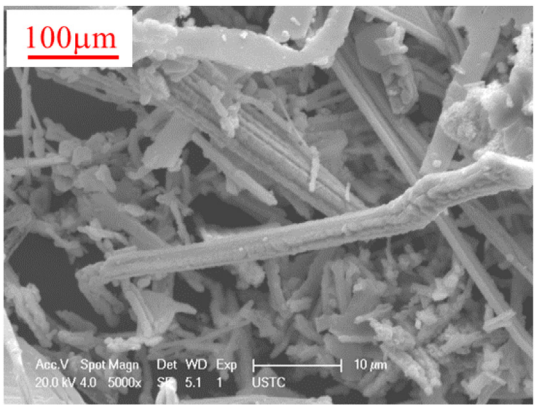

Fig. 10. The microstructure of the bouyant debris.

Figs. 13(c) and 12(c). The solubility of the Cu element changes with the temperature of liquid Li, but it is constant in liquid Li held at 620 K. In theory, for solubility-driven dissolution, the flux (J), of one type element into liquid metal, in units of $g \cdot m^{-2} \cdot s^{-1}$, can be expressed as follow [33–35]:

$$J = k \times (A_0 - A), \tag{2}$$

where k is the transfer coefficient in units of $g \cdot m^{-2} \cdot s^{-1}$, A_0 is the solubility of the element in a liquid metal, and A is the actual concentration of the dissolved element. It has been demonstrated that the solubility of copper in Li is less than 5×10^{-3} at.% [36]. As listed in Table 1, the actual concentration, A, of Cu in Li is 0.001%. Eq. (2) can be simplified as follow:

$$J = k \times C, \tag{3}$$

where C is difference between the A_0 and A, it's a constant. Thus, J also is a constant. According to Eq. (3), the mass loss of the nine specimens in present experiment can be written as:

$$\Delta W = \sum_{i=1}^{9} J \times S_i \times t, \tag{4}$$

where S_i, in unit m^{-2}, is surface area of the number i specimen, t is the corrosion time in unit s. In fact, for solubility-driven dissolution, corrosion will be stop when the concentration of element is saturated in liquid metal. The maximum value of theoretical weight loss of nine specimens is about 7 g upon an assumption of 5×10^{-3} at.% as the saturation concentration of Cu in static liquid Li, which is far less than 85 g.

In isothermal, all-liquid systems, equilibria can generally be achieved after some period of time, and corrosion stops when solubility relationships are satisfied. However, the equilibrium may be upset by the presence of a second metal. In isothermal systems, when two or more solid metals or alloys are in contact with a common liquid metal, mass transfer can occur between the metals, even though the solubilities of those particular metals in the liquid metal are small [37,38]. Additionally, there are two types of mass transfer in isothermal liquid metal system. First, the solid metals dissolve into liquid metal, and these solid metals atoms are transferred to and deposited on the surface of another metal, resulting in weight loss of one metal and weight increase of the other. Second, the compounds or alloys are formed either by elements of both metals, or by elements within the liquid metal. These compounds may then be deposited into the liquid metal, leading to mass loss of the solid metals. In the present experiment, the ratio of Li volume V_{Li} (cm^3) to the total surface area S (cm^2) of Cu specimens and 304 SS are 32 cm and 2 cm respectively. Thus, the isothermal mass transfer must be occurred in the experiment. No compounds or alloys are formed by Cu and the constituent elements of 304 SS in liquid Li at 620 K, and it is also not possible to form Cu–Li alloys under the experimental conditions. Therefore, the most probable form of mass transfer of Cu in liquid Li is that dissolved Cu atoms, are transferred to the surface of 304 SS, and deposited on the wall of

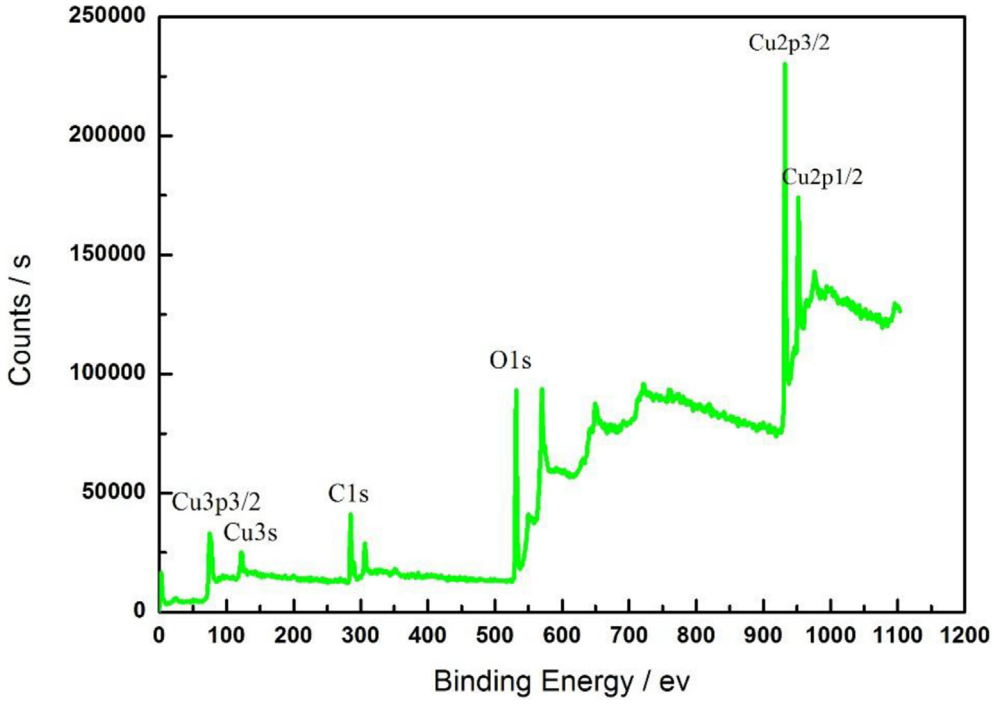

Fig. 11. XPS analysis result of the buoyant debris.

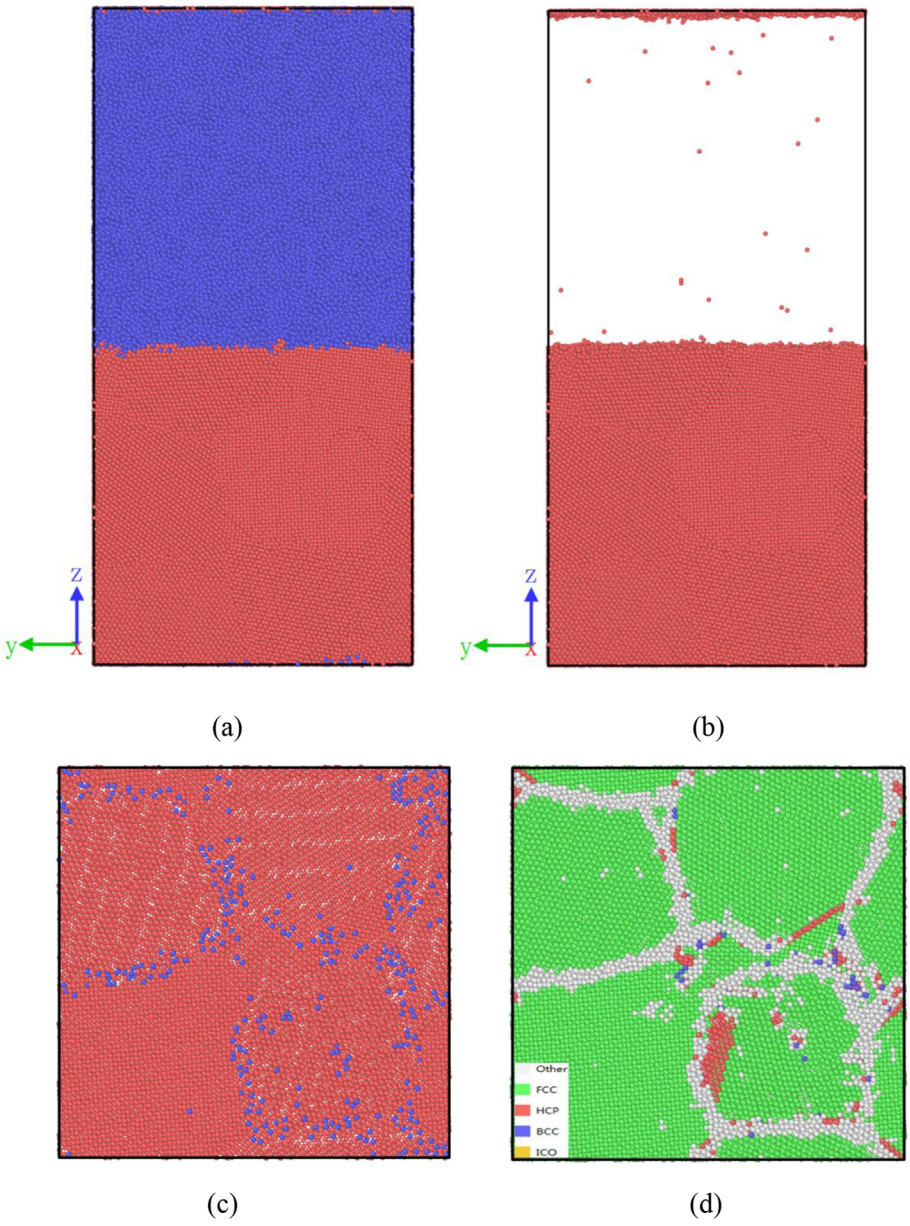

Fig. 12. The snapshots of the equilibrated solid-liquid system after a relaxation time of 1.0 ns. (a) the solid-liquid interface, (b) Cu substrate after deleting Li atoms, (c) Cu substrate section, the red spheres represent Cu atoms and the blue spheres represent Li atoms, (d) the CNA results of the Cu substrate section, the white region corresponds to the grain boundaries. (For interpretation of the references to colour in this figure legend, the reader is referred to the Web version of this article.)

test vessel. However, after cleaning, there was no significant deposition of Cu discovered on the wall of test vessel, as shown in Fig. 14. This result suggests that, at most, only a small amount of dissolved Cu atoms could have been transferred to the surface of 304 SS, thereby indicating that there are other reasons for the large Cu mass loss other than physical dissolution and mass transfer.

For the second corrosion mechanism, liquid Li permeates into surface layer of the specimen through grain boundaries. The permeated Li atoms act like a wedge, which will expand the width and depth of the marks and grains boundaries, as shown in Fig. 7(b), subsequently resulting in the tilted edge of both the through hole and hollow, as shown in Figs. 4 and 5. In addition, as shown in Fig. 13(d), when the permeated Li from the grain boundaries form a closed circuit under the surface layer of the specimen, the affected layers (Cu debris) with spearhead and metasequoia leaf shapes will disassociate from the specimen surface, drop into the liquid Li, and eventually fall to the bottom of the test vessel. This process is responsible for significant Cu mass loss from the specimen. As a result of this mass loss, more grain boundaries have been further exposed to the liquid Li, as shown in Fig. 7(c). During this dissolution of Cu into the liquid Li, the Cu debris can be further decomposed into smaller particles and the grains begin to assume a pebble shape through continued physical dissolution and intergranular corrosion, as shown in Figs. 7(d) and 9. However, if the permeated Li do not form a closed circuit loop under the surface layer of the specimen, these layers will remain adhered to the specimen substrate, as shown in Fig. 6(c). Because this type of corrosion is significantly enhanced when additional grain boundaries exposed to liquid Li, these Cu specimens were seriously damaged by this type of large-scale Li attack, as shown in

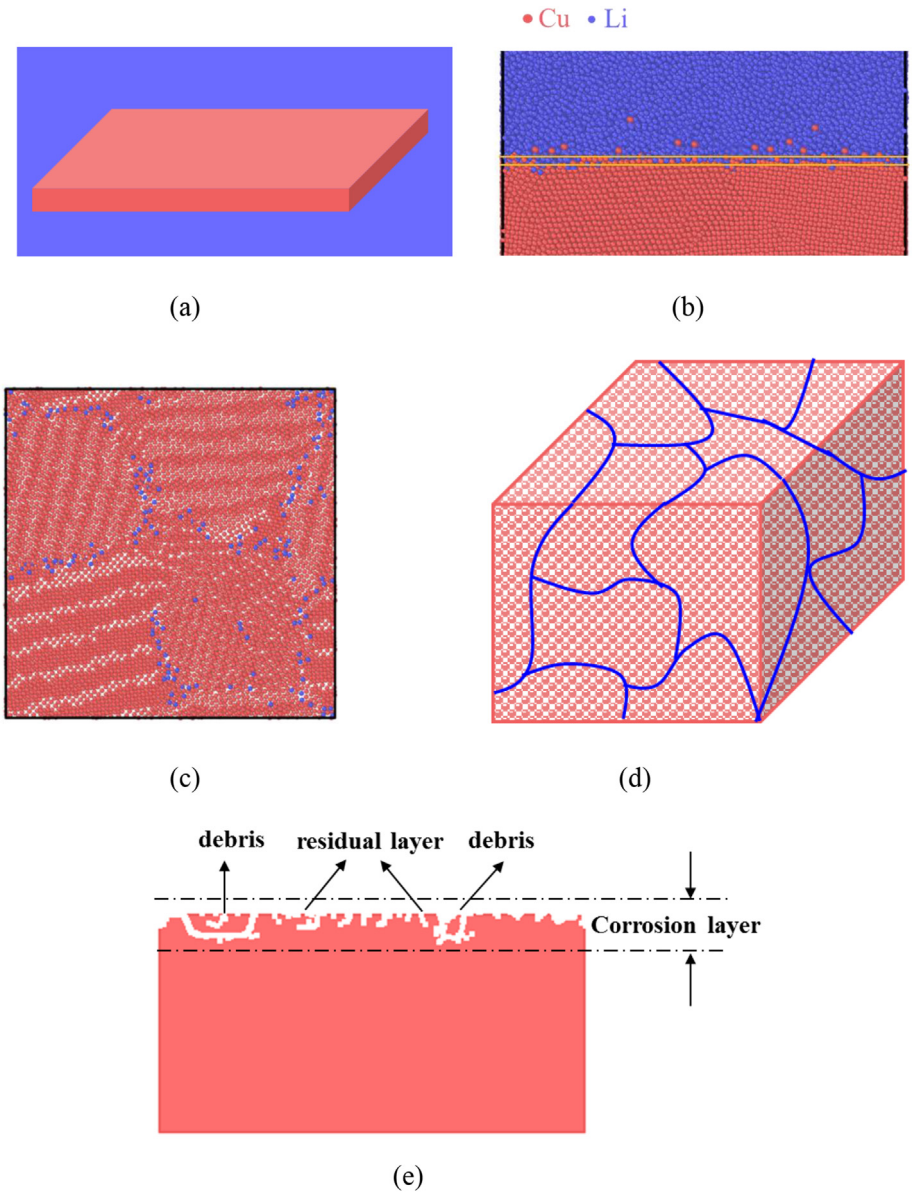

Fig. 13. The graphs of the corrosion mechanisms. (a) initial state, (b) Cu element dissolves into liquid Li from the specimen near the solid-liquid interface, (c) the cross-section of Cu–Li solid-liquid interface, (d) liquid Li permeates into the surface layer of the specimen through the machine marks and grain boundaries, (e) the cross-section of the specimen after corrosion by liquid Li.

Fig. 13(e). Therefore, grain boundary corrosion appears to be the primary mechanism for weight loss and surface damage of the specimens.

When the remnant Li, which contained Cu debris and atoms, was cleaned with water, the Li reacted violently with the water, released both of heat and hydrogen (H_2), and oxidized some of the Cu. The relevant chemical reaction that occurred is:

$$2x\,Li + y\,Cu + (2x + y)\,H_2O \xrightarrow{\Delta} 2x\,LiOH + yCuO + (x + y)\,H_2\uparrow. \quad (5)$$

Under the effect of the H_2, the Cu oxide became porous, buoyant, and floated to the water surface, as shown in Figs. 10 and 11. The residual Cu which did not participate in the above chemical reaction remained on the bottom of the storage vessel.

However, one thing that should be considered is whether Cu specimen is oxidized and/or nitrified during the pumping and baking stage. Theoretically, the following reactions will occur when Cu specimens are baked:

$$Cu + N_3 \xrightarrow{\Delta} CuN_3, \quad (6)$$

$$4Cu + O_2 \xrightarrow{\Delta} 2Cu_2O \quad (7)$$

the Gibbs free energy of Eqs. (6) and (7) are −38.3 kJ/mol and −247.0 kJ/mol at 620 K, respectively. Cu is not completely oxidized because the vacuum pressure is about 10^{-4} Pa meanwhile the Cu is excess during baking stage. And the following reactions must occur in liquid lithium if the Cu is oxidized and/or nitrified because these reactions are spontaneous:

$$9Li + CuN_3 \rightarrow 3Li_3N + Cu, \quad (8)$$

Fig. 14. The test vessel after cleaning.

$$2Li + Cu_2O \rightarrow 2Li_2O + 2Cu, \quad (9)$$

the Gibbs free energy of Eqs. (8) and (9) are −669.4 kJ/mol and −792.0 kJ/mol respectively at 620 K. Thus, it is observed that the Cu oxide and nitride layer affect the corrosion process of Cu in liquid Li. The Cu atoms will dissolve into liquid Li and the Li atoms penetrate into the surface layer of Cu after the oxide and nitride layer are depleted. Due to the much higher vacuum level of the vessels, we did not detect the composition on the surface of the specimen after baking stage. However, we will verify whether this hypothesis is correct or not in future work.

5. Conclusion

The corrosion characteristics of Cu specimens in static liquid Li at 620 K under high vacuum conditions were investigated. It was found that the corrosion mechanisms of Cu in liquid Li under the given conditions of the experiment include two primary aspects: physical dissolution and intergranular corrosion. Cu dissolves into liquid Li from the specimen near the solid-liquid interface. Additionally, liquid Li permeates into surface layer of the specimen through machine marks and grain boundaries. Due to the low solubility of Cu in Li, solubility-driven physical dissolution is not the main reason for mass loss of specimens. When the permeated Li forms a closed circuit under the surface layer of the specimen, the closed-circuit layers will detach macroscopic Cu debris, which will enter the liquid Li from the corroded surface, which will result in significant Cu loss from the specimen. Thus, intergranular corrosion is the primary mechanism responsible for the weight loss and surface damage.

Finally, the “corrosion protection grade” of Cu in liquid Li reaches 10, which indicates that Cu cannot withstand the corrosion of liquid Li at 620 K under high vacuum. If liquid Li and Cu materials are simultaneously used in future fusion devices, it will be necessary to effectively isolate the Cu from the liquid Li and/or apply corrosion resistant coating material to the surface of the Cu components.

Acknowledgement

This research is funded by National Key Research and Development Program of China (2017YFA04025000 and 2017YFE030110), National Nature Science Foundation of China under the contract Nos. 11625524, 11775261, 11321092, 51371080, 11605246. The authors would like to acknowledge the support of the computation platform of National Super-Computer Center in Changsha (NSCC).

References

[1] Z.J. Ren, et al., A Practical Manual of Metal, first ed., Jiangsu Science and Technology Publishing House, Nanjing, 2007.
[2] Y.Z. Zhang, et al., Vacuum Materials, first ed., Metallurgy Industry Press, Beijing, 2005.
[3] W.B. Gauster, et al., J. Nucl. Mater. 212–215 (1994) 3.
[4] J.Y. Park, et al., Fusion Eng. Des. 83 (2008) 1503.
[5] M. Lipa, et al., Fusion Eng. Des. 75–79 (2005) 469.
[6] Y.T. Song, et al., Fusion Eng. Des. 85 (2010) 2323.
[7] Y.T. Song, et al., Fusion Eng. Des. 75–79 (2005) 499.
[8] D.M. Yao, et al., Fusion Eng. Des. 69 (2003) 355.
[9] G.N. Luo, et al., Phys. Scripta T128 (2007) 1.
[10] J.S. Hu, et al., Nucl. Fusion 56 (2016) 046011.
[11] S. Malang, et al., Fusion Eng. Des. 27 (1995) 399.
[12] T. Muroga, et al., Fusion Eng. Des. 61–62 (2002) 13.
[13] R. Majeski, et al., Nucl. Fusion 45 (2005) 519.
[14] A.A. Tuccillo, et al., Nucl. Fusion 51 (2011) 094015.
[15] S.V. Mirnov, et al., Plasma Phys. Contr. Fusion 48 (2006) 821.
[16] J.C. Schmitt, et al., Phys. Plasmas 22 (2015) 05611.
[17] M.A. Jaworski, et al., Nucl. Fusion 53 (2013) 083032.
[18] J.W. Coenen, et al., Phys. Scripta T159 (2014) 827.
[19] G.Z. Zuo, et al., Nucl. Fusion 57 (2017) 046017.
[20] Z. Yao, et al., Fusion Eng. Des. 81 (2006) 2887.
[21] M. Kondo, et al., Fusion Eng. Des. 87 (2012) 1777.
[22] S. Plimpton, et al., J. Comput. Phys. 117 (1995) 1.
[23] X. Chen, et al., Comput. Mater. Sci. 119 (2016) 114.
[24] Y. Shibuta, et al., Acta Mater. 105 (2016) 328.
[25] S. Nose, et al., J. Chem. Phys. 81 (1984) 511.
[26] W.G. Hoover, et al., Phys. Rev. 31 (1985) 1695.
[27] M. Parrinello, et al., Phys. Rev. Lett. 45 (1980) 1196.
[28] M.Q. Zhao, et al., Corrosion and Protection of Metals, first ed., National Defense Industry Press, Beijing, 2002.
[29] R.J. Pulham, et al., J. Nucl. Mater. 115 (1983) 239.
[30] Qi Xu, et al., J. Nucl. Mater. 394 (2009) 20.
[31] X.C. Meng, et al., J. Nucl. Mater. 480 (2016) 25.
[32] X.C. Meng, et al., Fusion Eng. Des. 128 (2018) 75.
[33] P.F. Tortorelli, et al., J. Nucl. Mater. 191 (1992) 965.
[34] M. Kondo, et al., J. Nucl. Mater. 417 (2011) 1200.
[35] M. Kondo, et al., Fusion Eng. Des. 86 (2011) 2500.
[36] J.N. Mundy, et al., Phys. Rev. B 8 (1973) 5477.
[37] J.R. Distefano, et al., J. Mater. Eng. 11 (1989) 215.
[38] M. Kondo, et al., Plasma Fusion Res. 8 (2013) 3405053.